Journal of Applied Polymer Science

Multiscale Approach to the Morphology, Structure, and Segmental Dynamics of Complex Degradable Aliphatic Polyurethanes

Milena Špírková, Luďka Machová, Libor Kobera, Jiří Brus, Rafał Poręba, Magdalena Serkis, Alexander Zhigunov

Institute of Macromolecular Chemistry AS CR, v.v.i., Heyrovského nám. 2, 162 06 Praha 6, Czech Republic

Correspondence to: M. Špírková (E-mail: spirkova@imc.cas.cz)

ABSTRACT: A multiscale approach spanning from the segmental (subnanometer) up to micrometer level was applied for detailed study of the self-assembly of aliphatic block polyurethane (PU) elastomers. To understand the principles of the self-organization of hard and soft segments in the complex multi-component systems, several two-component model PU samples, that is, the products of 1,6-diisocyanatohexane (HDI) with three diols differing in the length and constitution were also prepared, characterized, and investigated: (i) polycarbonate-based macrodiol (MD), (ii) biodegradable oligomeric diol (DL-L; product of butane-1,4-diol and D,L-lactide), and (iii) butane-1,4-diol (BD). The study (particularly ^{13}C-^{1}H PILGRIM NMR spectra) reveals complex internal organization and interesting (application appealing) behavior of multi-component PUs. Hard segments (HDI+BD products) feature self-assembled and significantly folded chain conformations with interdomain spacing 15–22 nm (small-angle X-ray scattering analysis). The small domains are hierarchically assembled in various structural formations of μm size (spherulites) depending on PU composition, as detected by transmission electron microscopy and atomic force microscopy. © 2014 Wiley Periodicals, Inc. J. Appl. Polym. Sci. **2015**, *132*, 41590.

KEYWORDS: elastomers; nanostructured polymers; polyurethanes; self-assembly; spectroscopy

Received 25 July 2014; accepted 2 October 2014

DOI: 10.1002/app.41590

INTRODUCTION

Polyurethane (PU) elastomers, their blends and nanocomposites are very popular and frequently used polymeric materials thanks to broad versatility of their functional properties.[1–28] For a longer time, they have been amply used as automotive accessories, sport devices, in furniture, packaging, and so forth, but at present, they have also been tested in modern medical applications.[1–20] Although these materials have been attracting the interest of scientists and manufacturers for more than 6 decades, they are still appealing from the academic point of view, especially if a non-conventional combination of starting components have been used in PU formulation. Unfortunately, due to patented or blocked technologies, important pieces of information concerning the PU elastomers (PUEs), especially the chemical composition and processing procedures are often inaccessible for a broad research community.

PUs prepared from macrodiol, diisocyanate and chain extender ("short" diol) belong to typical thermoplastic elastomers (TPE). TPE materials feature the rubber-like behavior at regular temperature, but (unlike conventional, slightly chemically cross-linked rubbers) they can be processed and recycled like thermoplastics. Common thermoplastic polyurethanes (TPU) are linear multiblock copolymers containing soft segments formed by macrodiol and hard segments, the reaction products of chain extender with diisocyanate. Segmented TPUs typically exhibit a two-phase morphology as a result of the incompatibility between their hard and soft segments, which is very important for their (sometimes unique) properties. The versatility of these materials arises from a relative ease of varying their hard (HS) and soft segments (SS) content, their compositions and molecular weights. The segregation of hard and soft segments in TPUs is generally only partial and depends on chemical nature and structure of hard and soft segments, on the overall composition, processing conditions, and on thermal treatment. To understand the functional properties of novel synthesized TPUs (including the structure-property relationship), a detailed multidisciplinary study of the structure and behavior spanning from the segmental (nanometer) scale up to macroscopic level is necessary.

Nowadays, biocompatible PUs are used also as degradable biomaterials in medicine, for example, as soft or rigid temporary scaffolds in tissue engineering,[3,8,10,11] provisional materials in surgery (self-absorbing sutures, stents, etc.),[4,7] or as drug release systems.[6,12–14] Artificial scaffolds employed in tissue engineering and regenerative medicine should have mechanical properties resembling those of the healthy target tissue in order to avoid

or minimize unwanted inflammatory reactions. As the elastic moduli of natural tissues vary from units of kPa (e.g., in brain) to units of MPa (e.g., in bone tissues), a broad choice of mechanically suitable elastomers is desirable for different tissue regeneration and other applications.

The development of synthetic degradable materials with appropriate mechanical and targeted functional properties (suitable compatibility, non-toxicity, high surface area, tailored degradation speed from weeks to years) is the focal point of material science, especially in the last decade.[2,8,11,12,16–20] Degradable polymeric materials are not only interesting as potential biomaterials for applications in medicine and related branches, but they are suitable candidates replacing the non-degradable plastics accumulating in the environment. They are promising materials from the environmental point of view, because their degradability can be tuned in the interval of days up to years, depending on their intended use.

Numerous degradable synthetic polymer materials are based on polyesters because the ester group is apt to the degradation process. Polyesters and PUs based mainly on polycaprolactone, L-, D- or D,L-lactic acid (or lactide), and glycolic acid (resp. glycolide) and their copolymers have been widely tested and used in medicine as biomaterials.[1–4,8,10,11,14–17,20,25,29,30] Low-molar mass oligomers containing ester groups, end-capped by hydroxyl groups (M_n mostly between 1000 and 3000), serve as macrodiols in PU synthesis.[28] Although their low resistance against degradation properties is suitable for the time-limited (environment-friendly) applications, the end-use properties (particularly mechanical properties) are often poor. In order to improve desired functional properties, miscellaneous PU blends or multicomponental PU systems have been prepared and investigated.[4,8,25]

Polycarbonate (PC) diols—mostly in combination with aromatic diisocyanates—are more and more exploited macrodiols in PU synthesis,[20–27] especially for preparation of PU-based biomaterials with suitable mechanical properties and good biocompatibility. Recently, a series of segmented, aliphatic PC-based PUEs and their nanocomposites with excellent mechanical properties and hydrolytic resistance was prepared and characterized.[21–24] As a second step extending the previous study, novel degradable PC-based PUs with suitable mechanical properties were synthesized and characterized in detail. A short degradable oligomeric diol (synthesized specifically for this purpose) was used together with the PC-based macrodiol in the synthesis of degradable PUs, in contrast to commonly used polyester-based macrodiols. The strategy aimed at the preparation of multicomponent PUs made from PC-based macrodiol, degradable oligomeric diol, butane-1,4-diol (BD), and diisocyanate allowing the preparation of targeted samples with relatively regularly distributed degradable ester units in the linear PU chain. PU chain is formed by two hydroxyl components contributing to the soft segments (macrodiol and oligomeric D,L-lactide-based diol) and two components being prevalently considered as hard segments [BD and 1,6-diisocyanatohexane (HDI)]. The variation in PU composition has been achieved by changing the fraction of hydroxyl groups from individual diols, while the molar isocyanate-to-total-hydroxyl ratio was kept constant, equal to 1.05.

The presented contribution thus describes the synthesis and multilevel physicochemical characterization of the hierarchical self-assembly, segmental dynamics, structure and morphology of multicomponent PUs. The structure and behavior of the prepared PU systems at length scales spanning from individual molecular segments up to micrometer level by a combination of spectroscopy, microscopy, and scattering techniques was investigated. Specifically, solid-state NMR spectroscopy revealed extensive dynamical heterogeneities and dual dynamics of each component even in relatively simple model two-component PU systems consisted of diisocyanate and diol blocks. It was found out that HDI as well as BD form both relatively rigid and fairly flexible part of the PU chain, depending on their covalently bound neighbors. Moreover, as revealed by combining the X-ray scattering and microscopy techniques the hard segments self-assembly into the domains with interdomain spacing between 15 and 22 nm. These nanodomains further undergo self-aggregation into the micrometer-size formations.

The detailed description of macroscopic, namely thermal and mechanical properties of the multi-component PUs will be published in the separate contribution.[31]

EXPERIMENTAL

Materials

The commercially available reagents, PC-based macrodiol T5652 (kindly provided by Asahi Casei, Japan; number-average molar mass M_n = 2874 g mol^{-1}, dispersity $Đ_M$ = 3.23); BD, dubutyltin dilaurate (DBTDL), and HDI (all Fluka) were used. Oligomeric "degradable" diol unit (DL-L) was prepared by ring-opening polymerization of D,L-lactide in solution, initiated by BD in the presence of tin(II) 2-ethylhexanoate as catalyst. Detailed synthesis procedure is described elsewhere.[32] The isolated product was a pale yellowish, viscous liquid (M_n = 390 g mol^{-1}, $Đ_M$ = 1.28). The idealized schematic representations of structures of (a) PC-based diol (PC, composed of altering of odd C6 (hexamethylene) and even C5 (pentamethylene) units connected by carbonate groups) and (b) degradable DL-L diol are shown in the Figure 1.

Preparation Procedure

Since both PC and DL-L are viscous liquids, prior to the reaction all components were mixed in a thoroughly dried organic solvent in order to obtain homogenous solutions. After solvent evaporation, reaction mixtures were poured into the teflon molds and placed in an oven over the nitrogen atmosphere. All the reactions proceeded in bulk at 90°C for 24 h in the presence of DBTDL as the catalyst (50 ppm mol^{-1} of urethane groups) with a constant R ratio (R = [NCO]/[OH]$_{total}$ = 1.05). Changes in the sample compositions were achieved by the variations of molar ratios of hydroxyl groups ([OH]$_{total}$ = [OH]$_{PC}$ + [OH]$_{DL\text{-}L}$ + [OH]$_{BD}$). Individual sample codes and composition are summarized in Table I, columns 1–3. Hard segment content (HSC, Table I column 4) was calculated as the weight percentage of BD and HDI components with respect to the total mass of all reagents used for the particular sample preparation. The final thickness of the films was 250 ± 25 μm.

Methods of Characterization

NMR Spectroscopy. ^{1}H NMR spectra were recorded on a Bruker AVANCE DPX 300 spectrometer [Larmor frequency,

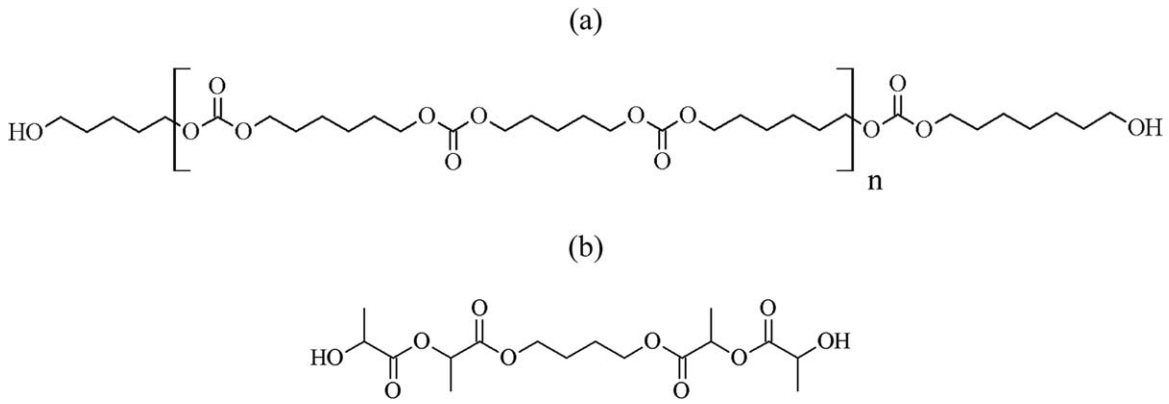

Figure 1. The structure of (a) PC-based diol (PC) and (b) degradable diol based on D,L-lactide (DL-L).

$\nu(^1H) = 300.131$ MHz] using a 5 mm multinuclear probe. The temperature of measurement was 300 K, and ^1H NMR chemical shift was calibrated using residual $CHCl_3$ signal (7.02 ppm). Solid-state NMR spectra were recorded on a Bruker AVANCE III HD spectrometer [Larmor frequencies $\nu(^1H) = 500.181$ MHz, $\nu(^{13}C) = 125.783$ MHz] using a 4-mm cross-polarization (CP)/magic angle spinning (MAS) probe. The ^{13}C NMR isotropic chemical shift was calibrated with glycine as an external standard (176.03 ppm; carbonyl signal). During the signal acquisition, high-power dipolar decoupling was used to eliminate strong heteronuclear dipolar couplings. The dried samples were placed into the ZrO_2 rotors and all NMR experiments were performed at 300 K. Frictional heating of the rotating samples was compensated using the procedure described in literature.[33]

The direct-polarization (DP) as well as CP/MAS NMR spectra were measured at spinning frequency of 11 kHz. The number of scans was 5120 for both ^{13}C MAS NMR and ^{13}C CP/MAS NMR experiments. The spin lock of 1.5 ms was used for ^{13}C CP/MAS NMR experiments and repetition delay was 4 s. The ^{13}C MAS NMR spectra were collected with 2 s repetition delay.

The ^{13}C-^1H PILGRIM NMR spectra[34] were measured at 12.5 kHz spinning frequency with the number of scans 160 per increment and recycle delay of 3 s. The nutation frequency of the $B_1(^1H)$ field for on-resonance cross-polarization and LG irradiation in SEMA recoupling sequence was $\omega_1/2\pi = 75$ kHz with resonance offset +53 kHz.

FTIR Spectroscopy. The FTIR spectra were recorded on a Perkin–Elmer Paragon 1000PC FTIR spectrometer using the reflective ATR (Attenuated total reflection) technique Specac MKII Golden Gate Single Reflection ATR System with a diamond crystal with the angle of incidence 45°. The samples were directly put on the diamond crystal and measured. All spectra were measured at wavenumber range 4400–450 cm^{-1} with resolution 2 cm^{-1} and with 16 scans. Software Spectrum v2.00 was used for processing the spectra.

Small-Angle X-ray Scattering. Small-angle X-ray scattering (SAXS) experiments were performed using a 3 pinhole camera (Molmet/Rigaku) attached to a multilayer aspherical optics (Osmic Confocal Max-Flux) which monochromatizes and concentrates the beam of a microfocus X-ray tube (Bede) operating at 45 kV and 0.66 mA (30 W). The camera was equipped with a multiwire, gas-filled two-dimensional (2D) detector with an active area diameter of 0.2 m (Gabriel design). In the high resolution mode the sample to detector distance was 2.24 m and in the low resolution mode 0.41 m, so that total interval from 0.043 to 10.5 nm^{-1} of the scattering vector magnitude $q = (4\pi/\lambda)\sin\theta$, where $\lambda = 1.54$ Å is the wavelength and 2θ is the scattering angle, could be reached.

Atomic Force Microscopy. Investigation of the topography and heterogeneity relief (PU films were previously freeze-fractured at the temperature of liquid nitrogen) was done by the atomic force microscope (Dimension Icon, Bruker), equipped with the SSS-NCL probe, Super Sharp SiliconTM-SPM-Sensor (Nano-SensorsTM Switzerland; spring constant 35 N m^{-1}, resonant frequency = 170 kHz). Measurements were performed under ambient conditions using the tapping mode atomic force microscopy (AFM) technique. The scans covered the sizes from 1 × 1 to 50 × 50 μm^2.

Transmission Electron Microscopy. Ultrathin sections of the films were cut at low temperature (sample temperature −80°C, knife temperature −50°C) using an ultramicrotome with cryo attachment (Ultracut UCT; Leica). The sections were transferred to supporting Cu grids and observed using a transmission electron microscope (TEM; Tecnai G2 Spirit; FEI). The TEM micrographs were taken in bright field imaging mode at 120 kV;

Table I. Codes, Composition, HSC, and SAXS Peaks Maximum Positions

Code	Molar ratio $[OH]_{PC} : [OH]_{DL\text{-}L} : [OH]_{BD}$			HSC (wt %)	SAXS $_{max.}$ (nm)
PU-1-0-1	1	0	1	16.0	21.6
PU-1-1-0	1	1	0	14.6	-
PU-1-1-1	1	1	1	21.9	19.9
PU-1-2-1	1	2	1	24.1	15.5
PU-1-1-2	1	1	2	28.1	15.8

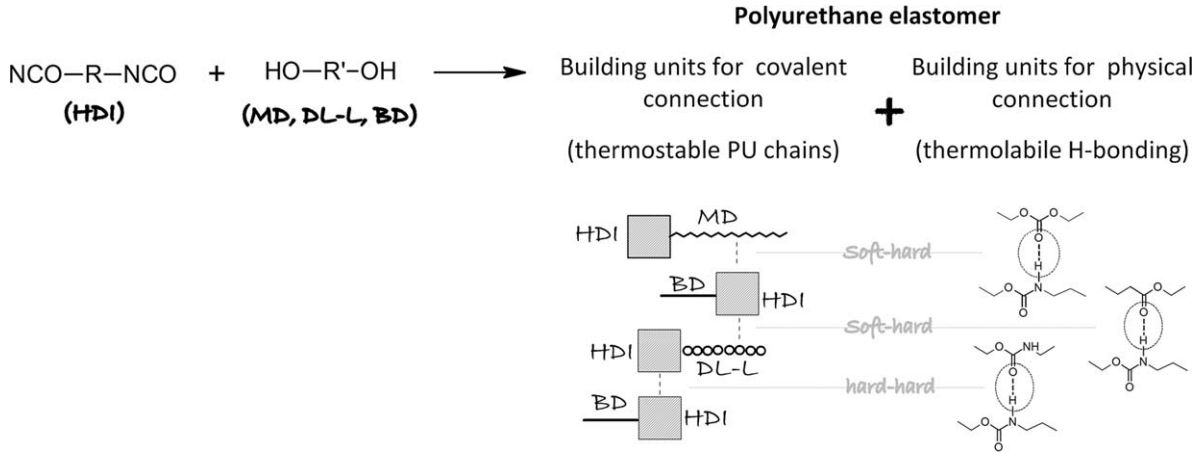

Figure 2. Basic building units for PUE formation.

under these conditions, the micrographs showed darker crystalline aggregates and dark particles in the lighter polymer matrix.

Scanning Electron Microscopy. Surface microstructure of PU films was measured by scanning electron microscope (SEM) on the instrument Vega Plus TS 5135 (Tescan, Czech Republic). Before SEM analysis, PU films were sputtered with 4 nm Pt layer using vacuum sputter coater SCD 050 (Balzers, Czech Republic).

RESULTS AND DISCUSSION

A series of novel segmented PUE films containing degradable DL-L and PC-based macrodiol units in the polymer backbone was successfully prepared by one-step procedure. The building units of PUE (connected either by covalent or physical bonds) are given in Figure 2. The strategy of the synthesis aims at degradable PU samples containing the segregated hard and soft domains and exhibiting suitable thermomechanical properties. The soft segments are relatively long and flexible. Their soft character originates from certain mishmash between the structure and arrangement of building MD and DL-L units differing in the chain constitution and length (for details, see Materials section). The hard segments are formed by the reaction of BD with HDI. They are structurally uniform and strongly interact with analogous units of neighboring chains (hard–hard segment interactions). It is why they allow for more regular and compact packing. Interactions of hard segments (-HN- unit) with carbonyl groups of either macrodiol or oligomeric diol are also possible (hard–soft segment interactions).

One of the mains goals of the study is the degradability of prepared samples. This influenced the choice of reactants. While the PC-based macrodiol secures good tensile properties of PUEs,[21,23] oligomeric DL-L diol represents the degradation center of the PU chain. The synthesized and studied PU chains are reaction products of diisocyanate with three diols, that is, they contain linear sequences made from MD+HDI, DL-L+HDI, and BD+HDI units connected by thermostable covalent bonds. Linear chains are further interconnected by thermolabile hydrogen bonds >N—H ... O=C<. While the hydrogen bonding >NH groups always belong to urethane units, >C=O groups belong either to macrodiol or DL-L, or to urethane. PU structure results in the "pseudo" covalent network interconnected by hydrogen bonds with parts of chains segregated in two types of domains (Figure 2). Because the structure of the multicomponent PU system is very complex, the two-component model polymers (i.e., the products of the polyaddition reaction of HDI with either PC diol, or DL-L or BD) were prepared, characterized, and studied for comparison.

The Liquid-State NMR Characterization of Degradable D,L-Lactide-based Diol

The NMR spectroscopy was used mainly for studying the structure and ordering of the prepared four-component PUs with a degradable D,L-lactide-based block. Although, the characterization of D,L-lactide building units (diol) using solution-state ^{1}H NMR spectroscopy was performed at first*.

The ^{1}H NMR spectrum of synthesized DL-L diol is shown in Figure 3. The characteristic chemical shifts of **a** and **b** signals can be assigned to CH_2 groups of the BD, the signals **c** and **d** are related to the CH_3 and the CH groups of the lactide inner units, and the chemical shifts **e** and **f** can be assigned to the CH and the CH_3 groups of the end lactide units, respectively. The signal **g** is attributed to hydroxyl groups. The molar mass, M_n, was calculated from the obtained ^{1}H NMR spectrum according to the formula:

$$M_n = \left(\frac{I_d}{I_e} + 1\right) \times 72 \times 2 \times 90$$

where I_d and I_e are the areas of peaks **d** and **e**, respectively, 72 is the molar mass of a DL repeat unit, and 90 is the total molar mass of the end part of the molecule.[35] Calculated M_n of DL-L resulted in value 380 g mol^{-1} that confirmed origins of DL-L monomer unit and it is with very good agreement with GPC analysis (Materials section).

Solid-State NMR Characterization of PU Systems

Two four-componental PU samples, PU-1-1-1 and PU-1-1-2, were chosen for a set of solid-state NMR experiments.

*Other components, 1,6-diisocyanatohexane (HDI), butane-1,4-diol (BD), and polycarbonate-based macrodiol were characterized by solid-state NMR spectroscopy in our previous work.[22]

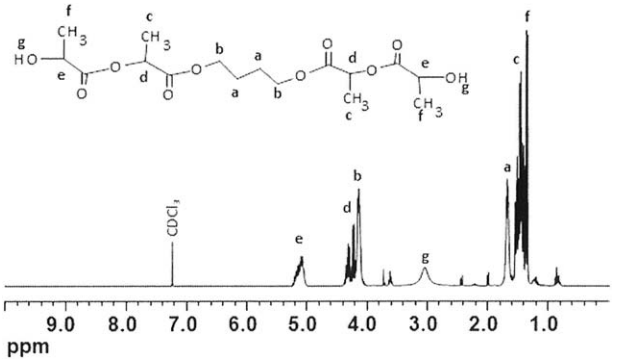

Figure 3. ^{1}H NMR of D,L-lactide-based diol (DL-L).

DP ^{13}C MAS NMR spectra were measured first. Applying the relatively short repetition delay (2 s) the measurement preferentially detects NMR signals of highly flexible polymer segments. The ^{13}C MAS NMR spectra of PU-1-1-1 and PU-1-1-2 systems do not indicate any significant differences in the flexible part of the PU sample [Figure 4(a)]. Subsequently standard cross-polarization ^{13}C CP/MAS NMR spectra were measured that allowed to detect ^{13}C NMR signals of rigid and semi-flexible components [Figure 4(b)].

In contrast to ^{13}C MAS NMR, clear differences between PU-1-1-1 and PU-1-1-2 were found in ^{13}C CP/MAS NMR spectra: a pronounced increase of broad signals at about 66, 43, and 28 ppm is visible in the system PU-1-1-2 [Figure 4(b)]. Because the prepared systems PU-1-1-1 and PU-1-1-2 are (at least) four-component polymer systems, a set of model two-component PU was prepared to help the spectral interpretation and assignment of NMR signals. To increase the spectral resolution of overlapped ^{13}C NMR signals and to investigate local segmental motions in the prepared systems, the 2D ^{1}H-^{13}C PILGRIM NMR experiments allowing clear distinction of rigid and mobile segments were performed. In general, the rigid segments are characterized by broad doublets with the frequency splitting of about 13–10 kHz, while the mobile components exhibit narrow lines placed in the central part of the 2D ^{13}C-^{1}H PILGRIM NMR spectrum. Because the central signal reflects not only motionally averaged one-bond ^{1}H-^{13}C dipolar couplings, but also long-range ^{1}H-^{13}C dipolar couplings as well as imperfections in B_1 filed homogeneity the intensity of central resonances must be interpreted very cautiously.[36,37]

Therefore, the two-component system created from HDI and PC compounds was analyzed first. Although this system exhibits soft rubber-like macroscopic consistency, the obtained 2D ^{1}H-^{13}C PILGRIM NMR spectrum shows both the narrow central resonances and broad dipolar doublets. This indicates that the two-component PC-HDI system contains, in addition to the excess of flexible segments, considerable fraction of rigid domains (Figure 5). The data suggest (see also results of other techniques) that small-sized rigid domains are embed in soft polymer matrix. Because the ^{13}C NMR resonance at about 40 ppm attributed to HDI segments does not exhibit broad dipolar doublet, it is clear that the rigid domains are preferentially created from PC building blocks. This finding is slightly surprising because one would expect the opposite behavior. (In PUEs, diisocyanate block usually contributes together with the chain extender to the hard segments, featuring high rigidity of the system. In contrast, aliphatic PC diol as highly flexible compound forms the soft segments. However, in this system, formed solely from hexamethylene diisocyanate and PC

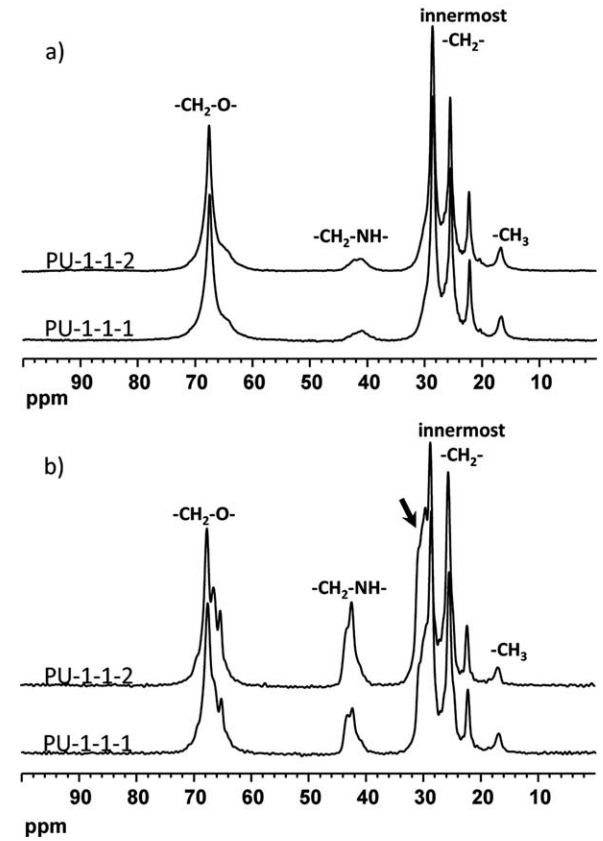

Figure 4. The ^{13}C MAS NMR spectra (a), and the ^{13}C CP/MAS NMR spectra (b) of four-component PU systems PU-1-1-1 and PU-1-1-2, respectively.

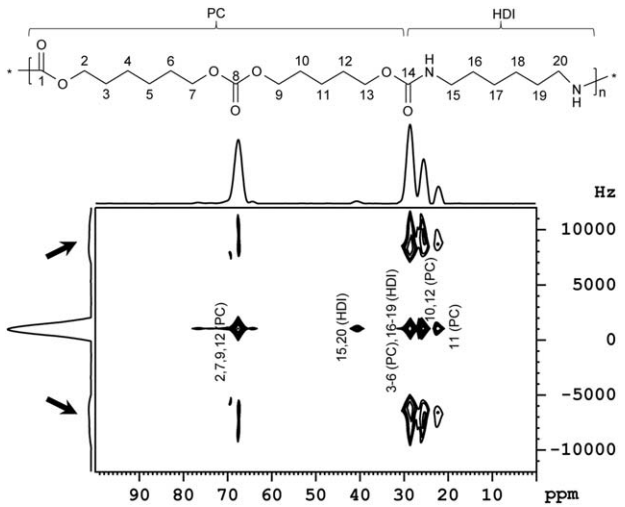

Figure 5. The structure and expanded part of 2D ^{1}H-^{13}C PILGRIM NMR spectrum of two-component systems created from PC and HDI blocks.

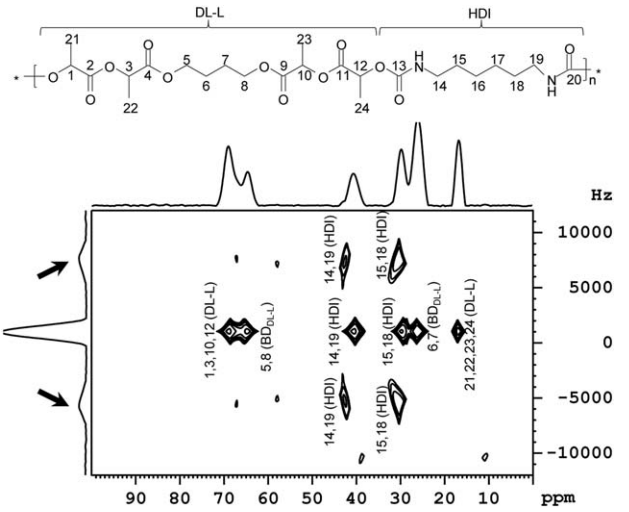

Figure 6. The structure and expanded part of 2D ^{1}H-^{13}C PILGRIM NMR spectrum of two-component systems created from DL-L and HDI blocks.

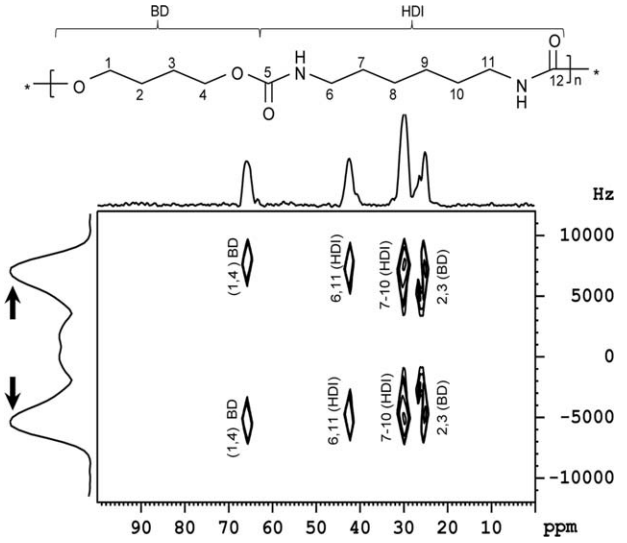

Figure 7. The structure and expanded part of 2D ^{1}H-^{13}C PILGRIM NMR spectrum of two-component systems created from BD and HDI blocks.

macrodiol, the more rigid regions are formed by PC macrodiol, whereas the diisocyanate blocks represent more flexible and mobile part of the system. It is supposed that part of PC segments adopt all-trans conformation that is stabilized by interchain non-covalent dipole–dipole interactions involving carbonate groups. With high probability these structural motifs undergo further self-aggregation and finally form nanosized domains).

Similarly, the second two-component system created from HDI and DL-L building blocks exhibiting honey-like consistency was analyzed. From the obtained 2D ^{1}H-^{13}C PILGRIM NMR spectrum it is obvious, that this two-component system contains soft and rigid segments as well. However, the flexible matrix is created from both DL-L and HDI segments in this case, while the rigid domains consist exclusively of HDI segments. As demonstrated by the splitting of the signal at about 40 ppm, the HDI segments form both rigid as well as flexible fraction of the prepared DL-L-HDI network. It can be supposed, that hard domains are formed during the reaction of diisocyanate with traces of water in DL-L leading to *N,N′*-dialkyl urea linkages (Figure 6).

At last the two-component powdered system composed from BD and HDI blocks was analyzed. In this case, the narrow central resonances are missing, indicating the absence of any considerable fraction of flexible segments. Both components BD and HDI thus form exclusively rigid domains that are reflected by the broad dipolar doublets (Figure 7).

In accordance with the interpretation of spectra of two-component systems, the assignment of resonance signals in the recorded 2D ^{1}H-^{13}C PILGRIM NMR spectra of the four-component PU-1-1-1 and PU-1-1-2 systems was performed. From the detailed analysis of corresponding 2D ^{1}H-^{13}C PILGRIM NMR spectra it is clear that hard segments are preferentially created by BD and HDI components (Figure 8). In contrast to two-component PC-HDI system the PC blocks are not involved in the formation of rigid domains and contribute to the creation of soft flexible polymer matrix. Substantial increase in the amount of hard segments was observed for the PU-1-1-2 (Figure 8). The order parameter S^2 calculated as the ratio of the motionally averaged dipolar couplings and the rigid-limit value (13.4 kHz) for HDI segments resonating at about 30 ppm revealed considerably higher ordering of rigid domains in the PU-1-1-2 system ($S^2 = 0.99$), while in the

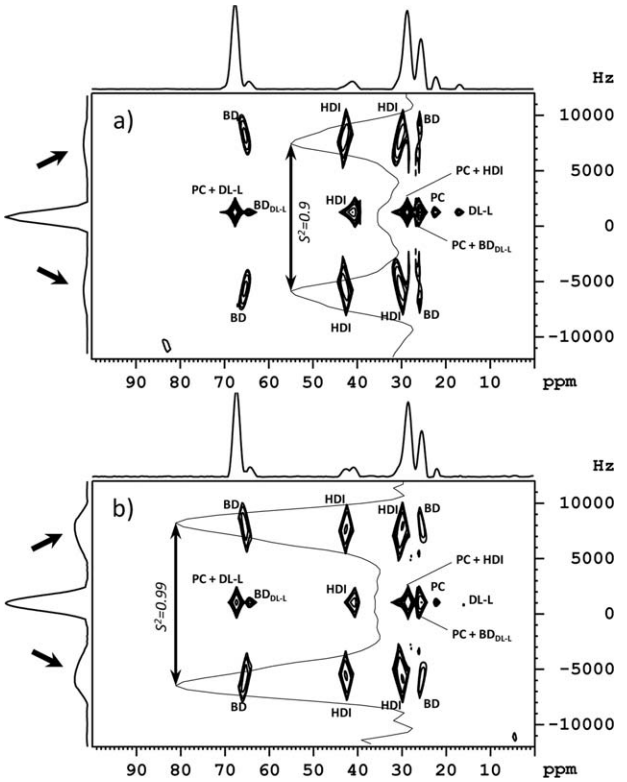

Figure 8. The expanded 2D ^{1}H-^{13}C PILGRIM NMR spectra of the prepared four-component systems PU-1-1-1 (a), and PU-1-1-2 (b) with the order parameters S^2 calculated for CH_2 units of HDI segments resonating at about 30 ppm.

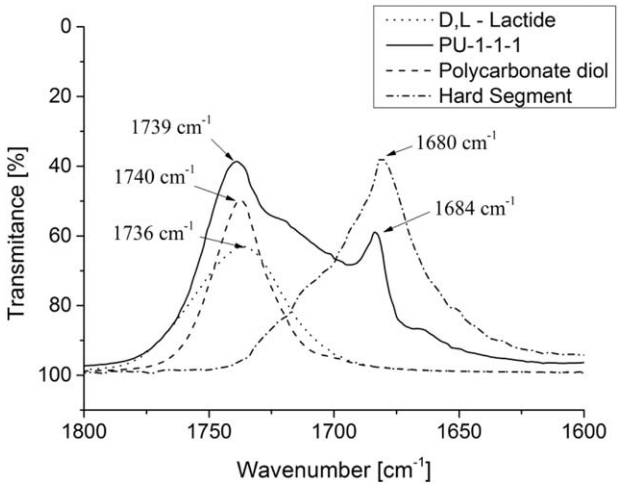

Figure 9. The detail of FTIR spectra of PC diol, DL-L, hard segment (HDI + BD product) and PU-1-1-1 in the carbonyl stretching region. Numbers indicate carbonyl peak wavenumbers.

system PU-1-1-1 residual segmental dynamics of rigid domains was found ($S^2 = 0.90$). It is worthy to note, that the HDI segments in the prepared four-component systems are present not only in rigid domains but partially also in soft polymer matrix. We assume that flexible HDI units are randomly incorporated between DL-L and PC blocks during the synthesis. Moreover, BD unit (BD_{DL-L}) used for the ring opening polymerization of D,L-lactide were found to act as an additional soft segment forming unit.

FTIR

FTIR was used for studying the conversion of isocyanate groups, chemical structure of PUs, and hydrogen bond formation in complex PU films containing relatively low HSC, between 15 and 28 wt. percentage.

First, we were interested if all isocyanate groups were consumed in the synthesis of complex PU products. Since the IR spectra of all synthesized products did not show any traces of the isocyanate peak at about 2270 cm^{-1}, we can conclude that a full -NCO conversion has been reached and no residual free isocyanate groups remain in prepared PU films.

Because the complex four-component PU samples are composed of soft segments (arising either from PC-macrodiol or oligomeric DL-L) and hard segments (HDI+BD reaction products), in which the hydrogen bonds between amino- and carbonyl-groups can be formed, the spectral region of carbonyl stretching vibrations from 1600 to 1800 cm^{-1} is the most interesting part of IR spectra. Figure 9 shows the part of IR spectra of carbonyl bands of building units of the PU chain together with spectra of PU1-1-1. The wavenumbers of all peak maxima are indicated in the Figure 9.

As the peak positions of free carbonyl vibrations in PC-macrodiol and in DL-L are almost identical (1740 and 1736 cm^{-1}), we assume that the most significant peak in PU at 1739 cm^{-1} belongs to the free carbonyl from the soft segment: However, IR does not discern if it concerns the carbonyl group from PC diol or from DL-L. The peak at 1684 cm^{-1} belongs to the carbonyl of urethane in the hard segment. Negligible difference between

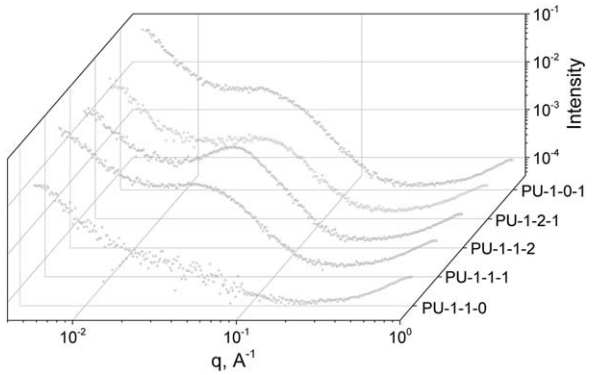

Figure 10. SAXS profiles of three- and four-component PUs. (Sample codes given in the figure are described in Table I).

peak positions in PU1-1-1 and in corresponding two-component model products (containing either "pure" soft or "pure" hard segments) shows that vibrations of groups in soft domains of PU-1-1-1 are not influenced by interactions with units from hard domains (and vice versa), which suggests a relatively strong domain segregation and relatively low content of H-bonds between units of hard and soft domains. The detailed FTIR study of analogous PUEs including the assignment of all peaks is given by Špírková et al.[22]

SAXS Experiments

To get additional pieces of information on the microphase-segregated structure, the SAXS experiments were performed. A number of papers indicate that homopolymers prepared merely from HDI and BD acquire folded-chain conformation that is also often present in PUs based on HDI/BD mixtures.[38,39] The important feature of aliphatic PUs is a closer proximity of the PU chains in the hard segment domains, as compared with aromatic PUs; the HDI/BD proximity (smaller distance between chain segments in the crystalline lattice and hence higher compactness) allows for further self-assembly of hard segments (via H-bonding) into domain/cluster patterns.[39] SAXS profiles of PU samples are shown in Figure 10. As

Table II. The Surface Roughness of Freeze-Fractured PU Films (Height Images 10 × 10 μm^2)

Code	Surface area (μm^2)	R_a^* (nm)	R_q^{**} (nm)	R_{max}^{***} (nm)
PU-1-0-1	107	209	133	1737
PU-1-1-0	100	17	14	149
PU-1-1-1	103	113	92	670
PU-1-1-2	101	97	74	669
PU-1-2-1	110	268	187	1735

Surface area: the total area of examined sample surface (the three-dimensioned area of a given region expressed as the sum of the area of all the triangles formed by three adjacent data points).
R_a^* (mean roughness): the mean value of the surface relative to the center place.
R_q^{**} (Rms): the standard deviation of the Z values within the given area.
R_{max}^{***} (max height): the difference in height between the highest and lowest points on the surface relative to the mean plane.
Mean: the average of all Z values within the enclosed area.

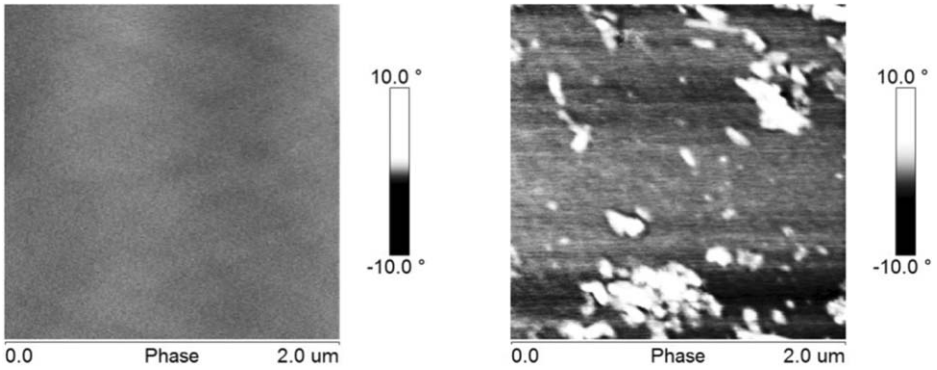

Figure 11. The comparison of the phase image of PU samples without any butanediol: PU-1-0-0 (left) and PU-1-1-0 (right).

expected, PU-1-1-0 prepared without any chain extender shows no scattering peak. All other PUs exhibit scattering peaks that are more (PU-1-1-2) or less pronounced (PU-1-0-1, PU-1-1-1 and PU-1–2-1). The values of interdomain spacing (calculated from the maximum peak position) are between 15.5 and 21.6 nm; the values increase with decreasing HSC (see Table I, 5th column). However, samples PU-1–2-1 and PU-1-1-2 have practically identical interdomain spacing in spite of different HSC. This phenomenon can be explained by the fact that hard blocks of different length can be found in PU chains. They can subsequently self-assemble into folded-chain conformations at lower HCS in more flexible PU-1–2-1 than for more rigid PU-1-1-2.

AFM and TEM

In the next part, the morphology and organization of PU films at larger (nanometer to micrometer) scales was studied. The AFM analysis of the surfaces of freeze-broken films was used for testing the "bulk" properties of PU films. Height images, that is, the topography of the samples of size 50 × 50 μm^2 (in the case of soft PU-1-1-0 only the scan 20 × 20 μm^2 was achievable) revealed that the reliefs of all PUs tested are very similar to each other and rough, like in our previous AFM results.[22] The only exception is the flat surface of the very soft sample PU-1-1-0. Surface roughness extracted from height images 10 × 10 μm^2 (not shown here) is given in Table II. It follows from Table II, that R_a and R_q values are of the order of magnitude 10^1 to 10^2 nm—unlike of R_{max} (which are 10^2 to 10^3 nm). The topography (roughness) of PU samples depends mainly on the presence/absence of BD in PU formulations, but any systematic trend on larger scales (exceeding the nm scale) reflecting the sample composition and complexity (e.g., three vs. four-component system and hydroxyl-component ratio) was not found—most probably, because the interplay of different interactions occurs at short distances and results in formation of segregated hard nanodomains immersed in a continuous softer matrix. The presence and content of nanodomains stabilized by non-bonding interactions and hydrogen bonds strongly influence the functional properties, for example, thermomechanical properties, degradability, etc. (as it will be shown in the next paper[31]), but the formation of nanodomains, which are more or less continuously dispersed in softer matrix does not almost affect the topology on micrometer and larger scales. Hence, we

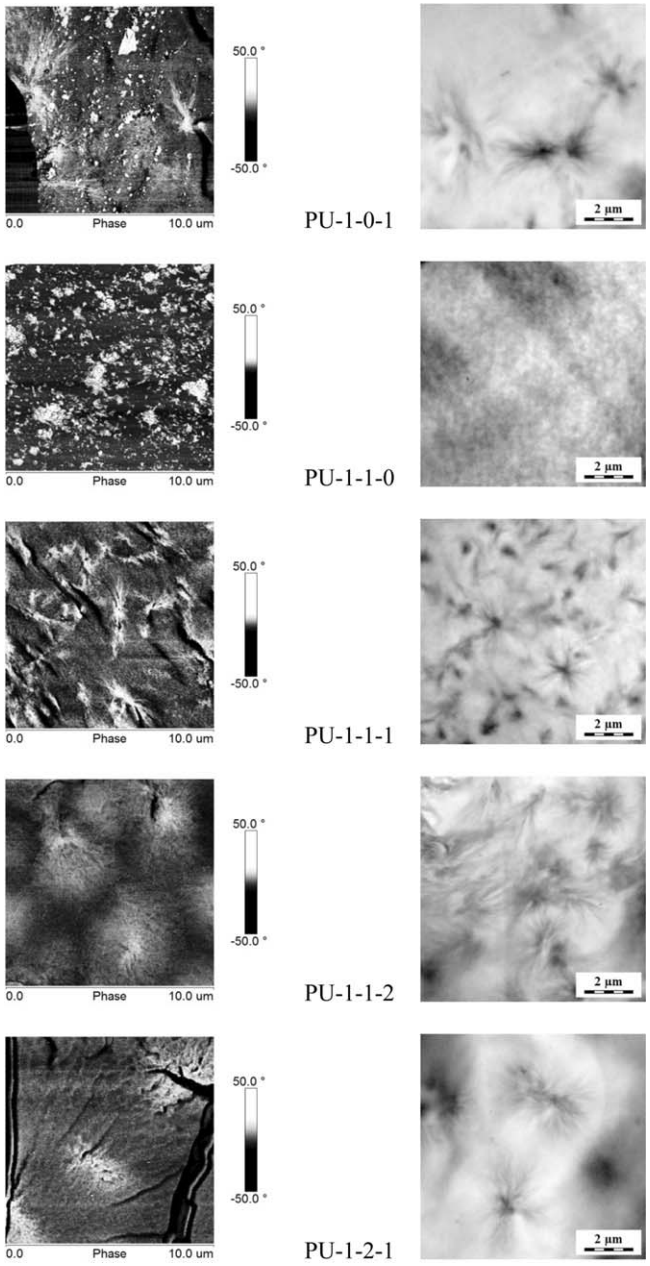

Figure 12. The comparison of AFM (left) and TEM (right) analyses. For sample codes, see Table I.

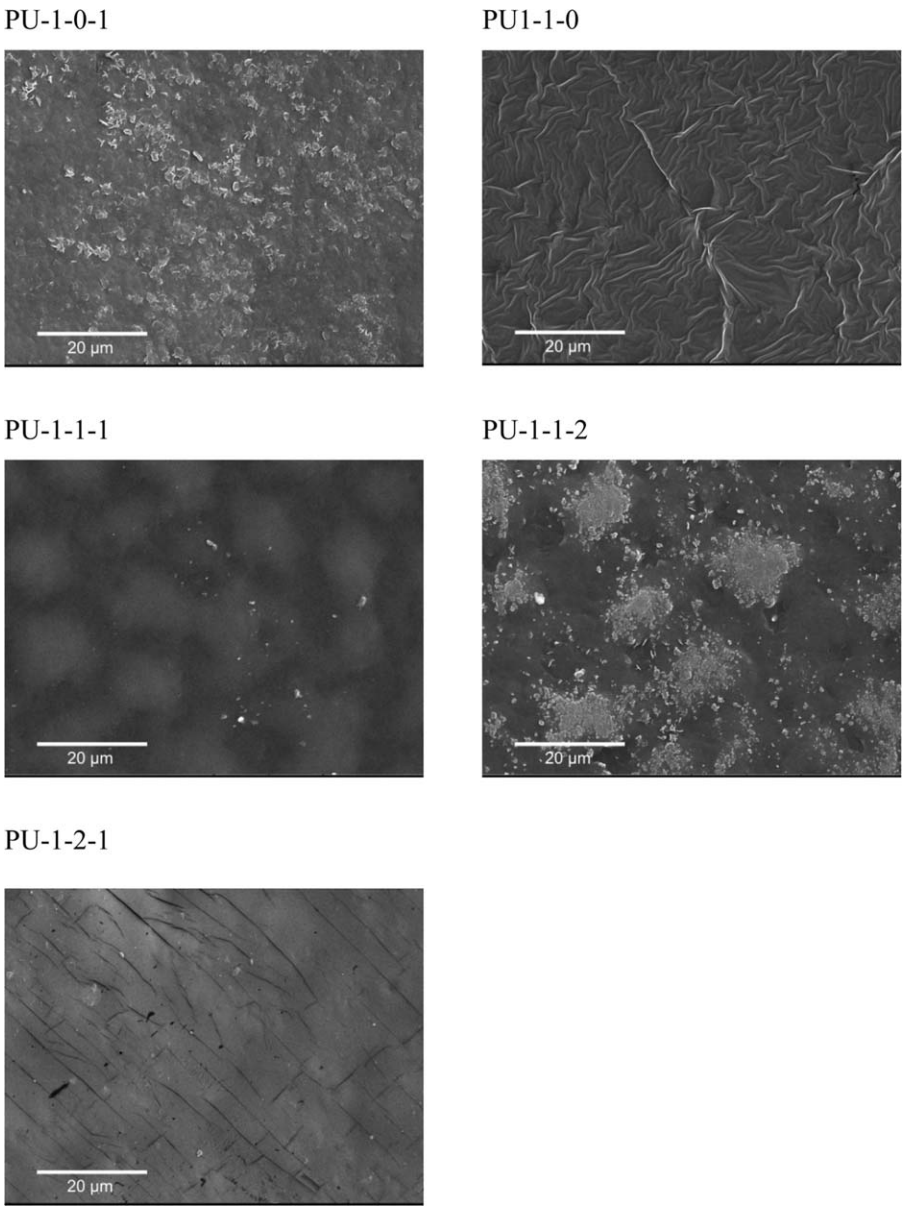

Figure 13. Surface relief of PU films (for sample codes see Table I).

can conclude that the microscopy study on micrometer scale supports the assumption concerning the nanostructure of prepared PUs.

Unlike the relative similarity of height images used for topological characterization of individual samples, phase images, which reflect the summarized (average) tip-sample interactions, yield significant information on bulk properties of complex PU films and provide qualitative heterogeneity mapping. The images show that PU-1-0-0, containing only macrodiol and HDI, is homogeneous (Figure 11) on the nm scale. In contrast, a distinct two-phase structure is evident in the case of PU-1-1-0 sample which contains also DL-L. Both the fairly small spherical formations (ca. 40 nm in diameter) and elongated aggregates up to the length about 500 nm and width about 250 nm are very well visible (bright formation in the Figure 11). As the color intensity of the darker region for sample PU-1-1-0 is very similar to that for PU-1-0-0, we assume that the bright portion in Figure 11 (right) originates from DL-L, which means that PU-1-1-0 is composed of (segregated) PC diol-rich and DL-L-rich nanometer-scale regions.

AFM phase images of three and four componental PU samples containing BD revealed the presence of spherulite formation of about 3 μm in diameter (unlike PU-1-1-0, prepared without any BD). Spherulites are products of the hierarchical self-assembly of nanometer-size structures in hard-segment domains (detected by SAXS) in larger micrometer-size formations. The AFM phase images were further compared with TEM images of cryo-cut samples with the almost identical magnification (Figure 12). The agreement of TEM and AFM size and shape analysis of nanometer and micrometer formations is excellent (Figure 12): it clearly shows that while PU-1-0-1 and PU-1–2-1 contains individual spherulites, the spherulite structures in PU-1-1-2

(containing the highest amount of hard segments) are interconnected. The PU-1-1-1 sample contains besides spherulites also vermicular formations.

SEM

SEM analysis of three- and four-component PU samples revealed different surface film relief on the micrometer scale (Figure 13). The relief reflects diverse self-assembly of nanodomains further arranged into different self-aggregated micrometer-size formations: The most flat and regular surface was found for PU-1-1-1, while very soft sample PU-1-1-0 is characterized by wrinkled surface morphology with the irregular fibrilar structure. All samples prepared with BD are heterogeneous on the μm scale (the more BD, the more distinguish surface heterogeneity). Samples PU-1-0-1 and PU-1-1-2 are rugged – "scaly" formations of μm size are evident. While the "scales" are homogeneously distributed on the surface sample PU-1-0-1, PU-1-1-2 film is obviously heterogeneous—irregular circle formations up to size 10 μm are clearly noticeable. Surface of the sample PU-1–2-1 is flat and it is distinguished by evident scratches and cracks.

CONCLUSIONS

A series of segmented thermoplastic PUs containing three diols in PU backbone (differing in the structure and length) was prepared by one-step procedure. FTIR confirmed the high conversion of functional groups. PU chain is formed by two hydroxyl components contributing to the soft segments (macrodiol and oligomeric D,L-lactide-based diol) and two components being considered as hard segments (BD and HDI). Solid-state NMR spectroscopy revealed significant complexity of PU systems due to different properties of two soft-segment compounds (i.e., oligomers differing in structure and chain lengths). However, the behavior of HDI itself (the hard-segment contributor) is not simple at all, as detected by PILGRIM NMR spectra. It can form either fairly flexible or relatively rigid part of PU chain, depending on the type of hydroxyl component connected with. The behavior of the last structure unit, BD also depends on its covalently bound neighbors: for example, BD unit inside DL-L chain contributes solely to the flexible part of PU while the reaction product of BD with HDI forms exclusively the rigid domains.

All PUs containing BD feature the self-assembly of hard segments into hard-segment domains with the interdomain spacing between 15.5 and 21.6 nm. The hierarchical self-assembly further generates micrometer-size formations: all PU samples studied exhibit distinct spherulite structures of about 3 μm size as detected by TEM and AFM. PUs prepared without BD differ in the homogeneity on the nm scale: while the PU made solely from macrodiol and diisocyanate is homogeneous, distinct heterogeneous character of macrodiol plus D,L-lactide-based diol plus diisocyanate on the nm scale was detected by AFM. The surface relief depends on the sample composition; the most regular and flat surface has the sample containing equal molar amounts of hydroxyl groups of all diols. Multi-component PUEs can be used as temporarily mechanically resistant, but simultaneously degradable coatings and films.

ACKNOWLEDGMENTS

The Authors wish to thank the financial support of the Grant Agency of the Czech Republic (Czech Science Foundation, project No. 13–06700S). The experimental work of Dr. D. Kubies (DL-L synthesis), J. Hromádková (TEM), and E. Miškovská, Jr. (SAXS) is acknowledged as well.

REFERENCES

1. Li, G. I.; Li, D. D.; Niu, Y. Q; He, T.; Chen, K. C.; Xu, K. T. *J. Biomed. Mater. Res. A* **2014**, *102*, 685.
2. Guelcher, S. A.; Srinivasan, A.; Dumas, J. E.; Didier, J. E.; McBride, S.; Holinger, J. O. *Biomaterials* **2008**, *29*, 1762.
3. You, Z. W.; Wang, Y. D. In Biomaterials for Tissue Engineering Applications: A Review of the Past and Future Trends; Burdick, J. A.; Mauck, R. L., Eds.; Springer: Wien, **2010**; p 75.
4. Zhao, X. W.; Ye, L.; Coates, P.; Caton-Rose, F.; Martyn, M. *Polym. Adv. Technol.* **2013**, *24*, 853.
5. Yari, A.; Yehaneh, H.; Bakhshi, H.; Gharibi, R. *J. Biomed. Mater. Res. A* **2014**, *102*, 84.
6. Paris, R.; Marcos-Fernandez, A.; Quijada-Garrido, I. *Polym. Adv. Technol.* **2013**, *24*, 1062.
7. Hearon, K.; Nash, L. D.; Volk, B. L.; Ware, T.; Lewicki, J. P.; Voit, W. E.; Wilson, T. S.; Maitland, D. *J. Macromol. Chem. Phys.* **2013**, *214*, 1258.
8. Mercado-Pagan, A. E.; Kang, Y. Q.; Ker, D. F. E.; Park, S.; Yao, J.; Bishop, J.; Yang, Y. P. *Eur. Polym. J.* **2013**, *49*, 3337.
9. Kuetting, M.; Roggenkamp, J.; Urban, U.; Schmits-Rode, T.; Steinseifer, U. *Expert Rev. Med. Devices* **2011**, *8*, 227.
10. Hsu, S. H.; Huang, S; Wang, Y. C.; Kuo, Y. C. *Acta Biomater.* **2013**, *9*, 6915.
11. Fu, S. Z.; Meng, X. H.; Fan, J.; Yang, L. L.; Lin, S.; Wen, Q. L.; Wang, B. Q.; Chen, L. L.; Wu, J. B.; Chen, Y. *J. Biomed. Mater. Res. A* **2014**, *102*, 479.
12. Shin, M. S.; Hong, J. Y.; Park, S. *J. Drug. Deliv. Sci. Technol.* **2012**, *22*, 301.
13. Saralegi, A.; Gonzales, M. L.; Valea, A.; Eceiza, A.; Corcuera, M. M. *Compos. Sci. Technol.* **2014**, *92*, 27.
14. Song, N. J.; Ding, M. M.; Pan, Z. C.; Li, J.; Zhou, L. J.; Tan, H.; Fu, Q. *Biomacromolecules* **2013**, *14*, 4407.
15. Eceiza, A.; Larranga, M.; de la Caba, K.; Kortaberria, G.; Marieta, C.; Corcuera, M. A.; Mondragon, I. *J. Appl. Polym. Sci.* **2008**, *108*, 3092.
16. Moravek, S. J.; Hassan, M. K.; Drake, D. J.; Cooper, T. R.; Wiggins, J. S.; Mauritz, K. A.; Storey, R. F. *J. Appl. Polym. Sci.* **2010**, *115*, 1873.
17. Tatai, L.; Moore, T. G.; Adhikari, R.; Malherbe, F.; Jayasekara, R.; Griffiths, I.; Gunatillake, P. A. *Biomaterials* **2007**, *28*, 5407.
18. Ma, Z. W.; Hong, Y.; Nelson, D. M.; Pichamuthu, J. E.; Leeson, C. E.; Wagner, W. R. *Biomacromolecules* **2011**, *12*, 2365.
19. Xu, Y. S.; Wu, X. Y.; Xie, X. Y.; Zhong, Y. P.; Guidon, R.; Zhang, Z.; Fu, Q. *Polymer* **2013**, *54*, 5363.

20. Baudis, S.; Ligon, S. C.; Seidler, K.; Weigel, G.; Grasl, C.; Bergmeister, H.; Schima, H.; Liska, R. *J. Polym. Sci. Part A: Polym. Chem.* **2012**, *50*, 1272.
21. Špírková, M.; Pavličević, J.; Strachota, A.; Poręba, R.; Bera, O.; Kapráková, L.; Baldrian, J.; Šlouf, M.; Lazić, N.; Budinski-Simendić, J. *Eur. Polym. J.* **2011**, *47*, 959.
22. Špírková, M.; Poręba, R.; Pavličević, J.; Kobera, L.; Baldrian, J.; Pekárek, M. *J. Appl. Polym. Sci.* **2012**, *126*, 1016.
23. Poręba, R.; Špírková, M.; Brožová, L.; Lazić, N.; Pavličević, J.; Strachota, A. *J. Appl. Polym. Sci.* **2013**, *127*, 329.
24. Poręba, R.; Špírková, M.; Pavličević, J.; Budinski-Simendić, J.; Szeczenyi, K. M.; Hollo, B. *Compos. Part B-Eng.* **2014**, *58*, 496.
25. Imre, B.; Bedo, D.; Domjan, A.; Schon, P.; Vansco, G. J.; Pukansky, B. *Eur. Polym. J.* **2013**, *49*, 3104.
26. Kojio, K.; Furukawa, M.; Nonaka, Y.; Nakamura, S. *Materials* **2010**, *3*, 5097.
27. Cipriani, E.; Zanetti, M.; Brunella, V.; Costa, L.; Bracco, P. *Polym. Degrad. Stab.* **2012**, *97*, 1794.
28. Hepburn, C. Polyurethane Elastomers, 2nd ed.; Elsevier Science Publisher LTD: England, **1992**.
29. Choi, N. Y.; Lendlein, A. *Soft Matter* **2007**, *3*, 201.
30. Zini, E.; Scandola, D.; Dobrzynski, P.; Kasperczyk, J.; Bero, M. *Biomacromolecules* **2007**, *8*, 3661.
31. Poręba, R.; Kredatusová, J.; Hodan, J.; Špírková, M. *J. Appl. Polym. Sci.* submitted.
32. Kricheldorf, H. R.; Kreiser-Saunders, I.; Boettcher, C. *Polymer* **1995**, *36*, 1253.
33. Brus, J. *Solid State Nucl. Magn. Reson.* **2000**, *16*, 151.
34. Hong, M.; Yao, X.; Jakes, K.; Huster, D. *J. Phys. Chem. B* **2002**, *106*, 7355.
35. Wang, W.; Ping, P.; Chen, X.; Jing, X. *Eur. Polym. J.* **2006**, *42*, 1240.
36. van Rossum, B. J.; de Groo, C. P.; Ladizhansky, V.; Vega, S.; de Groot, H. J. M. *J. Am. Chem. Soc.* **2000**, *122*, 3465.
37. Brus, J.; Urbanová, M. *J. Phys. Chem. A* **2005**, *109*, 5050.
38. Li, Y.; Ren, Z.; Zhao, M.; Yang, H.; Chu, B. *Macromolecules* **1993**, *26*, 612.
39. Mishra, A.; Aswal, V. K.; Maiti, P. J. *Phys. Chem.* **2010**, *114*, 5292.